Current control in ITER steady state plasmas with neutral beam steering

R. V. Budny[a)]
Princeton Plasma Physics Laboratory, Princeton, New Jersey 08543, USA

(Received 15 December 2009; accepted 17 February 2010; published online 23 April 2010)

Predictions of quasisteady state DT plasmas in ITER [R. Aymar *et al.*, Nucl. Fusion **41**, 1301 (2001)] are generated using the PTRANSP code [R. V. Budny, Nucl. Fusion **49**, 085008 (2009)]. The plasma temperatures, densities, boundary shape, and total current (9–10 MA) anticipated for ITER steady state plasmas are specified. Current drive by negative ion neutral beam injection, lower-hybrid, and electron cyclotron resonance are calculated. Four modes of operation with different combinations of current drive are studied. For each mode, scans with the negative ion neutral beam injection aimed at differing heights in the plasma are performed to study their effects on current control on the q profile. The time-evolution of the currents and q are calculated, and long-duration transients (up to $\simeq$1500 s) are predicted. Effects of the beam and alpha ion pressures on the magnetohydrodynamic equilibrium are predicted to significantly alter the bootstrap current. The TEQ equilibrium solver [L. Degtyarev and V. Drozdov, Comput. Phys. Rep. **46**, 481 (1985)] in PTRANSP is found to be much more accurate than the VMEC solver [S. P. Hirshman *et al.*, J. Comput. Phys. **87**, 396 (1990)]. Quasisteady state, strongly reversed q profiles are predicted for some beam injection angles when the current drive and bootstrap currents are sufficiently large.
 [doi:10.1063/1.3357353]

I. INTRODUCTION

Steady state plasmas are desirable for fusion reactors since the cycling of transient plasmas appears impractical for power generation. DEMO (Ref. 1) plans to rely on steady state plasmas. ITER (Ref. 2) plans to explore steady state scenarios having minimal inductive (Ohmic) current, since inductive currents cannot be sustained for long durations. One of the goals of ITER experiments will be to produce quasisteady state plasmas with a fusion gain Q_{DT} (defined as the ratio of the DT fusion and the external heating powers P_{DT}/P_{ext}) $\geq$5 for durations of up to 3000 s.

The heating and current drive systems for ITER plasmas are being designed. The primary systems being considered are the following: negative ion neutral beam injection (NNBI), ion cyclotron resonance frequency (ICRF), electron cyclotron resonance frequency (ECRF), and lower-hybrid current drive (LHCD).

Plasmas with conditions approximating steady state are being studied in various tokamaks such as JET[3,4] and DIII-D.[5–7] High performance quasisteady state plasmas have high confinement, normalized pressure β_n, and edge pressures, and low fractions of the Ohmic to total current. Often they also have reversed q profiles, with high values for q_{min}, and sometimes internal transport barriers (ITBs), i.e., regions with localized large gradients of the plasma temperatures.

There are indications from theory that the q and magnetic shear $\hat{s}$ profiles play important roles in determining turbulence, assumed to cause much of the energy, momentum, and species transport. Linear gyrokinetic simulations of ion temperature gradient and trapped electron mode turbulence indicate that the growth rate is proportional to $(\hat{s}-\alpha)/q$,[8] where α is the normalized pressure so that regions with large negative $\hat{s}$ and large q should have low transport. Nonlinear gyrokinetic simulations also indicate that the turbulence is strongly suppressed in regions with large negative $\hat{s}$. One paradigm is that turbulence originates in the edge region and spreads to the core unless there is a barrier between the core and edge to stop the spreading.[9] The barrier can be related to $(\hat{s}-\alpha)/q$.

Since the plasma current and q profiles have important roles in present experiments, ITER plans to control these using externally driven currents along with the bootstrap current, which is determined by the pressure profile.[10] The present plan for the initial phase of external heating in ITER DT plasmas is to include NNBI, ECRF, and ICRF. Also LHCD is being considered as a possible add-on.

Predictions of ITER steady state plasmas[11–14] have been made assuming that the energy transport is the sum of neoclassical and an additional *ad hoc* term depending on radius and shear. Above a power threshold, a sustained ITB is predicted with a reversed q profile. In Refs. 13 and 14 pure rf heating is assumed.

It is important to predict current and q profile control to assess the possibilities of achieving steady state plasmas. This knowledge can help design current drive and heating systems, and help plan for operating scenarios and diagnostics. Current drive predictions for ITER steady state and hybrid plasmas have been benchmarked.[15] Various codes for predicting current drive from NNBI, ICRF, ECRF, and LHCD were compared. Predictions from variety of transport codes were presented.

This paper uses the PTRANSP code[16–18] to generate time-dependent integrated predictions of steady state ITER plasmas. Profiles of current drive from NNBI, ECRF, LHCD, and the bootstrap current are calculated. The possibility of driving current with ICRF is not included. The total beam-

a)Electronic mail: budny@princeton.edu.

TABLE I. Summary of conditions and results (at 500 s) for the four modes studied. The applied powers for the current drive are listed. Additional power for heating might be needed to establish the plasmas. Additional heating does not change the computed currents or q since the plasma profiles are held fixed.

Mode of operation	Low-T	Low-T-ECCD	High-T	High-T-10
Flat top start time [s]	120	120	180	180
Flat top end time [s]	500	500	500	3000
Flat top $T_e(0)$ [keV]	22	22	33	33
P_{NB} [MW]	33	33	33	33
P_{LHCD} [MW]	10	10	30	30
P_{ECRF} [MW]	0	10	0	0
P_{DT} [MW]	300	300	485	485
Flat top β_n	2.3	2.3	3.6	3.6
Flat top I_p [MW]	9.0	9.0	9.0	10.0
Flat top I_{BS} [MW]	2.8–3.2	2.95–3.3	5.4–6.6	4.5–5.5
Flat top I_{NB} [MW]	1.3–2.1	1.3–2.25	2.3–3.15	2.0–3.1
Flat top I_{LH} [MW]	0.37–0.42	0.36–0.43	1.15	1.1–1.3
Flat top I_{EC} [MW]	0.0	0.55–0.56	0.0	0.0
Flat top I_{OH} [MW]	3.3–3.9	2.5–3.4	−0.8 to −1.9	0.6–1.3

driven current dominates those from ECRF and LHCD. In Refs. 13 and 14 beam current drive is not included.

The time dependence is important to model since the plasmas need to be formed transiently, and since they are also expected to have long duration transients during the flat top phase, such as those due to slow diffusion of the current profile and buildup of impurities such as alpha ash.

Also it is important to assess the magnetohydrodynamic (MHD) equilibrium magnetic flux surfaces of steady state plasmas since their equilibria are complex, and can be elusive. Disruptions are often encountered in present experiments. The constraint of MHD equilibrium will limit the operating space. This paper shows that the VMEC equilibrium solver,[19] commonly used for modeling, does not give accurate solutions for high performance steady state ITER plasmas.

Four modes of steady state DT plasma operation are considered, summarized in Table I. All have the standard toroidal magnetic field $B_{tor}=5.2$ T. Two have the nominal temperature profiles of the "reference scenario 4" steady state ITER regime, and two have higher temperatures to enhance the driven and bootstrap currents. For the first three modes, the total current is assumed to be 9 MA, and for the fourth, 10 MA. Various combinations of ECCD and LHCD are assumed. The NNBI is assumed to deliver $P_{NB}=33$ MW of 1 MeV D, and the vertical steering is scanned for each mode.

For many of the cases the predicted q profiles take long times to reach steady state. Some of the cases maintain current holes (regions with effectively infinite q near the magnetic axis) for long durations.

II. PLASMAS STUDIED

Currently PTRANSP is a fixed boundary code, so the boundary needs to be specified. Usually the evolution of the boundary shape just inside the separatrix is calculated using the TSC code.[20] Instead, for this work a fixed boundary is assumed. These are taken to be typical of the reference scenario 4 steady state regime.[11,21] The boundary is shown in Fig. 1.

Previous PTRANSP papers[16–18] use physics-based models to predict profiles of the temperatures T_e and T_i, and in some cases, the toroidal rotation v_{tor}. The models used are the GLF23 model[8,22] and the MMM08 model[23,24] (a modified version of Weiland model[25]).

These models predict H-mode plasmas with high P_{DT} when the pedestal temperatures (assumed as boundary values) are sufficiently high, but they have not yet succeeded in predicting, self-consistently, high performance steady state

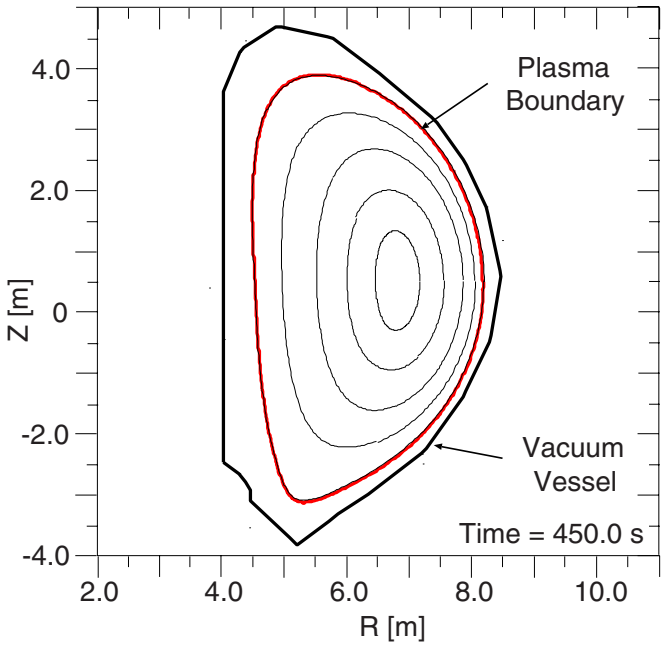

FIG. 1. (Color online) Plasma boundary and first wall assumed for all simulations. Internal flux surfaces computed for one of the High-T mode aimings (with Y=0.17 m).

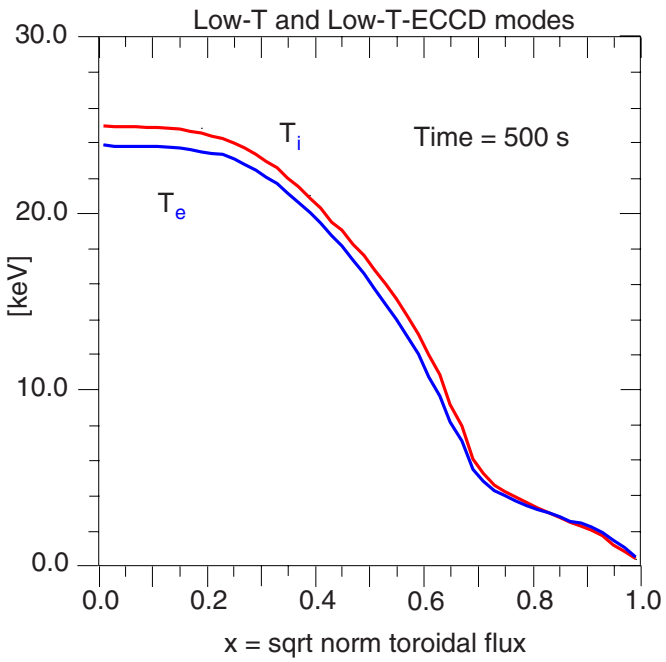

FIG. 2. (Color online) Assumed flat top temperature profiles for the Low-T and Low-T-ECCD modes.

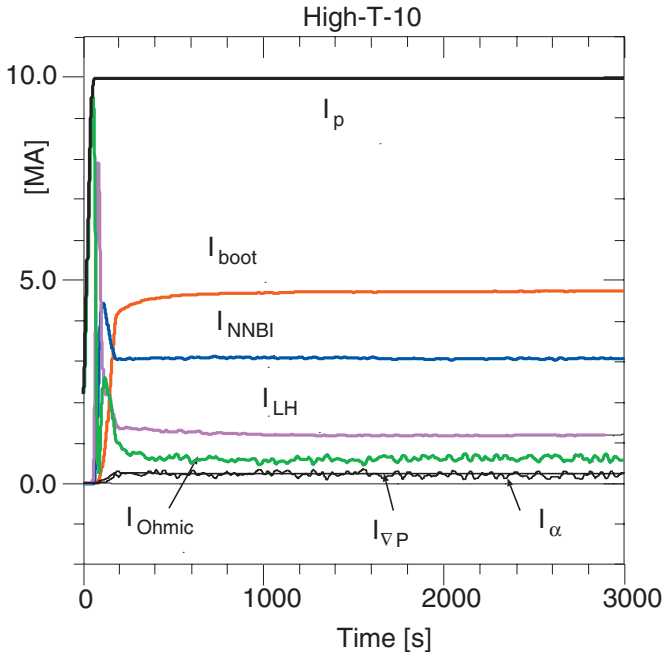

FIG. 3. (Color) Plasma currents for one of the High-T-10 mode aimings. The total is assumed to be 10 MA and the other currents are computed. Besides the dominant bootstrap, beam, and lower hybrid currents, small contributions from currents driven by the gradient of the pressure and the fast alphas are calculated.

plasmas for ITER. Very high pedestal temperatures ($\simeq$10 keV) may be required. The predictions are especially challenging due to the strong nonlinear coupling between current, rotation, temperatures, densities, heating, current drive, etc. Physics-based comprehensive predictive models have not been developed or tested well for this regime.

Since self-consistent predictions of steady state ITER plasmas are not yet reliable, canonical T_e and T_i profiles are assumed. The flat top temperature profiles for two sets of predictions, referred to as the Low-T and Low-T-ECCD modes are shown in Fig. 2. These profiles are typical of the ITER reference scenario 4 plasma.[21] They have the phenomenology of a weak ITB around x (the square root of the normalized toroidal flux, which is approximately the relative minor radius) =0.7. Another set of profiles is used for the High-T and High-T-10 mode aimings. Their temperature profiles are scaled up from the Low-T aimings by a factor of 1.5.

Since the temperature profiles are fixed the heating sources are not directly relevant. Changing the heating would change only the energy transport coefficients. The current drive profiles are crucial for predicting the current and q profiles. ICRF heating and current drive are ignored even though the heating might be needed to establish and maintain these steady state plasmas. Ranges of some plasma parameters for these four modes are summarized in Table I.

This use of PTRANSP with the plasma profiles being inputs is the same as the usual use of the TRANSP code in analysis mode. The heating, torquing, fueling, and current drive sources are computed. The radial flow of heat, angular momentum, particles, and flux are computed from the local conservation equations. The transport flows and coefficients are computed comparing these flows with plasma profiles and their gradients. This mode has also been used for predicting ITER performance.[26,27]

The total plasma current I_p consists of Ohmic I_{OH}, externally driven, and bootstrap I_{BS} currents. To study steady state plasmas in ITER, the plan is to reduce I_p from the standard 15 MA to $\simeq$9 or 10 MA in order to reduce the required Ohmic current (to near zero) and the external current drive. Here the driven currents are generated by NNBI, LHCD, and, in one scan, by ECRF. Total currents for one High-T case are shown in Fig. 3.

Since energy confinement increases with I_p in some plasma regimes, enhanced confinement appears needed to achieve high performance with reduced I_p. Plasmas with ITBs generally have enhanced confinement. One consequence of reducing I_p is that the density may need to be reduced. In present experiments the Greenwald fraction [$\bar{n}_e/\bar{n}_{GW}$ with $\bar{n}_e$ the line-average, and $\bar{n}_{GW} \equiv I_p/(\pi a^2) \times 10^{20}/\mathrm{m}^3$] needs to be around unity or lower for good confinement. The plan for the ITER baseline H-mode plasma is to limit the fraction at 0.86. For this study n_e is specified having Greenwald fraction 0.82 for the I_p=9 MA and 0.73 for the I_p=10 MA modes. The flat top profiles for DT plasmas are shown in Fig. 4. The temperature, density, and total current flat top start times are given in Table I. The effective charge Z_{eff} is held fixed in time and space at 2.17. Effects of impurity profiles and possible accumulation are ignored.

ITER plans to study steady state plasmas with durations of at least 500 s. As discussed in Sec. IV, for some of the scans, PTRANSP predicts that MHD equilibria cannot be maintained this long. Also transients in the current and q profiles are found lasting much longer than 500 s. To explore transient durations, some of the runs are extended to 3000 s.

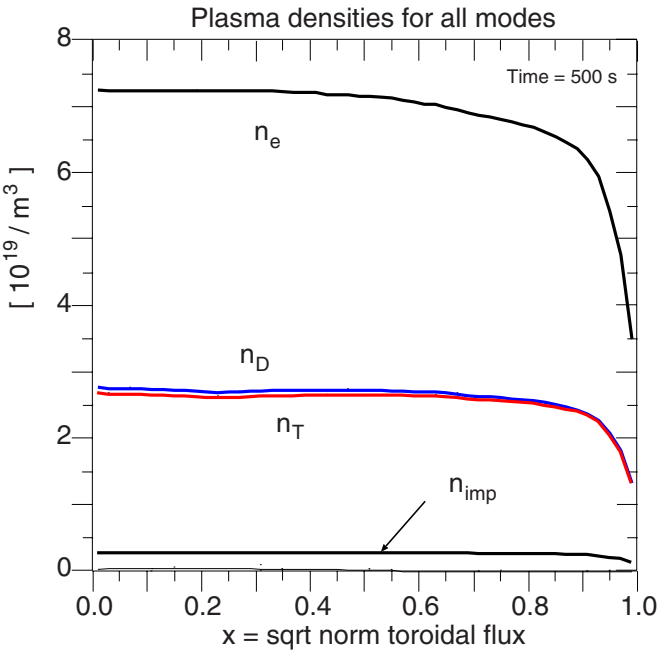

FIG. 4. (Color online) Assumed flat top density profiles. The n_e profile is assumed and the others are computed. A single impurity ion is assumed with Z=6, A=12, and Z_{eff}=2.17.

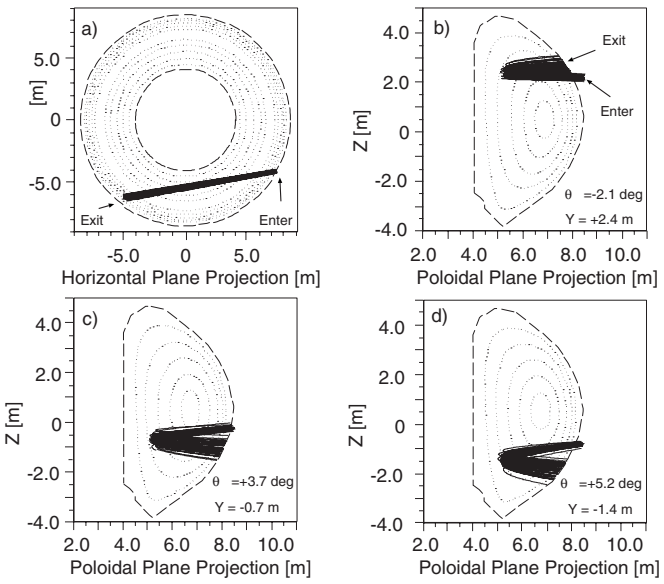

FIG. 5. Trajectories on NNBI neutrals with three different steering angles: (a) Horizontal view showing coinjection (parallel to I_p). (b) High steering with neutrals clustered around a height Z near +2.40 m at the minimum tangency radius. (c) Clustered near −0.68 m and (d) clustered near −1.40 m. The beam system and port ducts have not been finalized. The extreme upper and lower steerings are not compatible with the preliminary designs of the beam ducts unless the injectors are raised or lowered from their heights assumed here. The heights Y relative to the plasma magnetic axis are indicated.

III. EXTERNAL CURRENT DRIVE AND HEATING

The NNBI system has not been fully designed, but the plans are to inject D^0 at 1 MeV into DT plasma from two beam lines, each delivering 16.5 MW. The three-dimensional geometry used here is that with the small footprint cases of Ref. 16. Each source plane is modeled as a rectangle 0.56 m wide by 1.50 m high, located 30 m from the tangency radius, which is assumed to be 5.295 m. Each source plane is assumed to be elevated 1.34 m above the vessel midplane. The average height of the D^0 trajectories are planned to be adjustable by a rotation in the vertical plane of the NNBI sources. Presumably this rotation will be a complex operation, performed only rarely.

A wide range of aimings is considered. Examples of D^0 beam trajectories are shown in Fig. 5. The spreading shown in these plots results from the geometry of the sources and the assumed divergences and focal lengths. Aimings with upward steering are considered since there are potential advantages of upward injection.[28] The helicity of the magnetic field would shift the orbits and profiles of driven current, heating, and torque outward, and thus increasing their volume integrals. Upward aiming would be difficult to implement in ITER, since the beams must avoid structures such as the PF coils, and fit within the beam ducts. The height of the sources would have to be lowered. Also the extreme downward aiming would need the sources to be raised. These extremes are considered since they might be attractive possibilities for DEMO.

PTRANSP uses Monte Carlo methods[29,30] to calculate beam deposition, beam torque, as well as the slowing down, pitch-angle scattering, and thermalization of beam ions and fusion ions. For most of the simulations presented here, the number of Monte Carlo particles used for the beam ions is 5000 and for the alpha particles is 1000. These numbers of samples gives fairly smooth beam current drive (and heating profiles). A run with NUBEAM parallelized and 50 000 samples is discussed below. An example of the heating for one of the aimings is shown in Fig. 6. Effects which are not modeled here are the possible redistribution of fast ions by MHD, ripple, or anomalous diffusion.

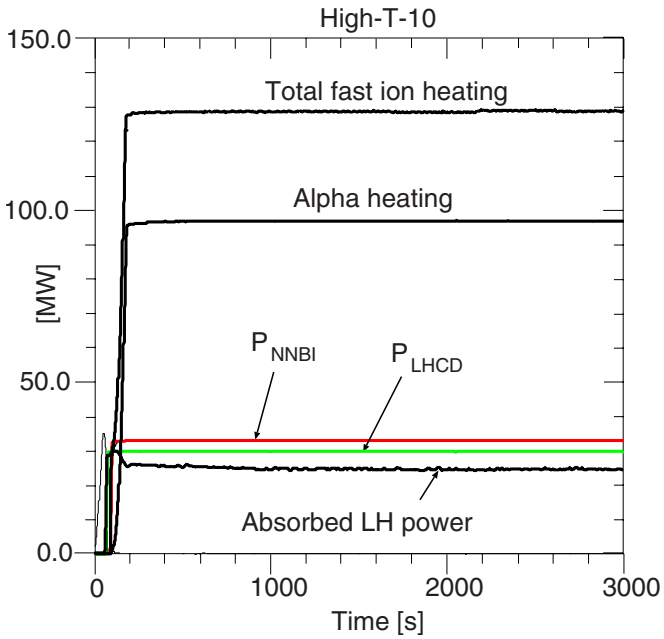

FIG. 6. (Color online) Heating for one of the High-T-10 mode aimings.

The planned LHCD frequency is 5.0 GHz. This is modeled using the LSC code,[31] using an adjoint method[32] for solving the Boltzmann equation. The spectrum of $n_{\|}$ is assumed to peak between 1.45 and 2.45. The subsidiary peak expected at negative $n_{\|}$ is ignored here, and is expected to add a negative peak to the drive current profile near $x=0.95$, and reduce the total current by about 30%. Benchmarking suggests that the LSC-predicted driven current is low due to the neglect of trapping effects. Thus the applied powers assumed here could over- or underestimate what is actually needed to yield the predicted LHCD profiles. The applied power for the Low-T and Low-T-ECCD modes is 10 MW and for the High-T and High-T-10 modes is 30 MW.

The planned ECRF heating and current drive frequency is 170 GHz, launched in O-mode. The TORAY code[33–35] is used to model the ECH/ECCD. One launching antenna near the vessel midplane is used, with toroidal angle assumed to be in the horizontal plane and aimed 30 degrees from the toroidal direction. TORAY launches 20 rays at each time step, and uses 251 radial zones. The ECCD is scaled up by a factor of 1.4 to account for momentum conserving effects not included in TORAY (Ref. 36). Synergistic effects of LHCD and ECCD, seen in present experiments,[37,38] and predicted to be small (<10%) in ITER plasmas,[12] are ignored here.

IV. PLASMA EQUILIBRIA

Solutions to the Grad–Shafranov equation are computed using the TEQ code[39] in PTRANSP. The inverse solver of TEQ is used for the fixed boundary solutions using the pressure and q profiles as input. The scaler MHD pressure used in PTRANSP-TEQ is computed as[40]

$$p_{mhd} = w_{th} + (4/3)w_{rot} + w_{par} + (1/2)w_{prp} \quad (1)$$

where $w_{th}(=n_eT_e+n_{th}T_i)$, w_{rot}, w_{par}, and w_{prp} are the energy densities of the thermal plasma, rotation, parallel fast ions, and perpendicular fast ions.

For the rotation contribution, the toroidal rotation of the bulk plasma is computed using the NNBI torque profiles and assuming that the ratio of the radial transport of the ion angular momentum and energy $\chi_{\mathrm{tor}}/\chi_i$ is 0.5. This predicts core rates of about 25 krad/s, implying very small contributions (less than 0.5%) to p_{mhd}.

Comparisons of the contributions to p_{mhd} for one of the modes are shown in Fig. 7. The contribution of the thermal plasma is nearly constant as the NNBI steering is scanned. Since the n_e, T_e, and T_i profiles are fixed, the only changes to w_{th} result from the changes in the fast ion dilution of the tritium and deuterium densities n_t and n_d.

The contributions of w_{par}, and w_{prp} to p_{mhd} are significant. Examples of their profiles for one of the steering cases are shown in Fig. 7. Most of the changes to $w_{par}+0.5w_{prp}$ with NNBI steering are due to changes in the beam ion profiles. The contributions to the volume-integrated $w_{par}+0.5w_{prp}$ from fast alpha ions are larger than those from the beam ions, but they change very weakly as the steering changes.

Some of the predictions discussed in Secs. V–VIII develop a "current hole," defined here operationally as the central q increasing above a preset limit value. PTRANSP cannot compute MHD equilibria when the profile of the total current becomes negative, so the maximum value of q is clamped numerically. Here q is clamped at 10, or as low as 7 in some runs that fail to maintain equilibrium solutions otherwise. It is not clear to what extent a current hole could be detrimental to plasma performance in ITER. Presumably the current drive could be feedback adjusted in time to avoid them.

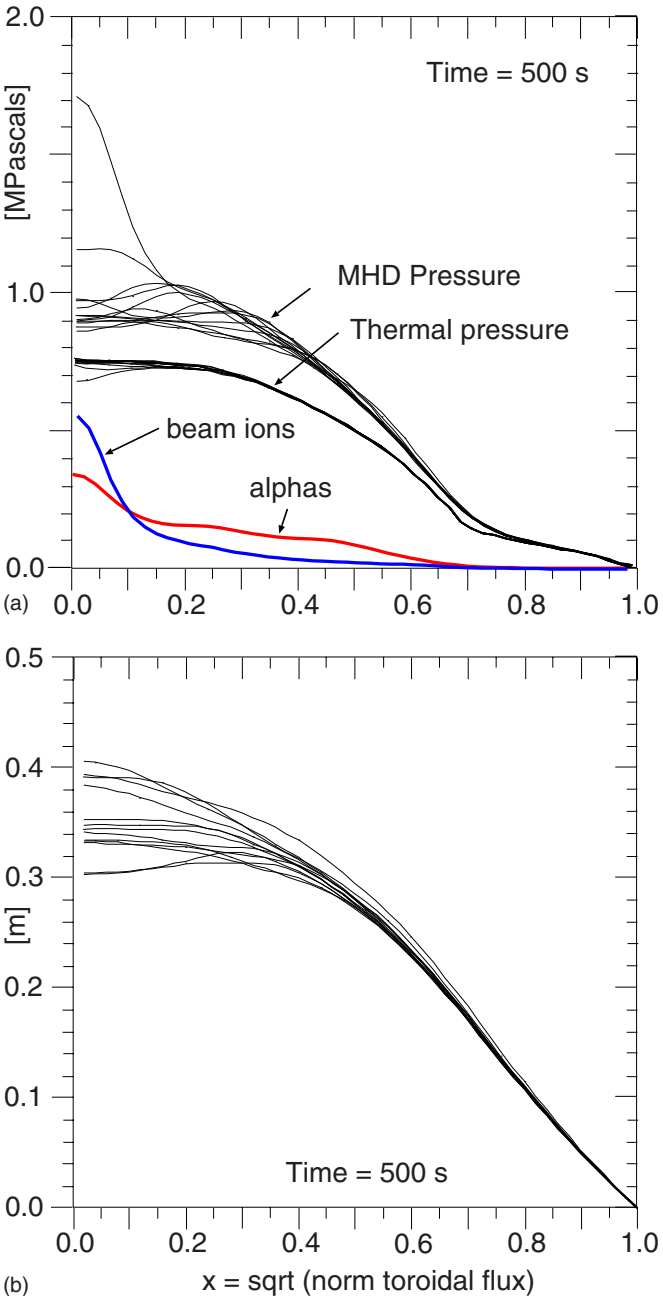

FIG. 7. (Color online) (a) Profiles of the thermal and MHD pressure profiles defined in Eq. (1) for the High-T-10 mode with various NNBI aimings. The contributions of the beam ions and alphas for one of the aimings (Y=+0.39 m and $\Delta \equiv$ Y−0.51 m) are shown. The beam contribution varies with the aiming as discussed below, whereas the alpha contribution does not vary. (b) Profiles of the Shafranov shifts.

Various name list options are available for controlling TEQ. One set of options fixes the number of radial and po-

loidal points used internally in TEQ. Either 151 or 251 radial points and 127 or 201 poloidal points are used here. These are adjusted to extend the discharge time in cases where failure to maintain equilibrium is encountered. (The number of radial zones used for the plasma profiles is 50.)

Another option selects the free parameters matched in the Grad–Shafranov solution. One of three choices is used here (to maximize the simulation duration when numerical failure is encountered): (1) q and the value at the edge of F =Major radius times B_{tor}; (2) as in (1) but with a loop to match plasma current by perturbing the q profile near the edge; and (3) surface-average of the parallel current $\langle\langle j \cdot B_{tor}\rangle\rangle$ and the value at the edge of F.

Another set of options controls the smoothing of profiles. For several of the predictions the plasma profiles needed to be smoothed over an interval ($\delta x = 0.05$) in order to maintain equilibrium. For some predictions the pressure near the axis had to be smoothed or dehollowed to maintain a Grad–Shafranov equilibrium solution.

Generally the resulting current and q profiles do not depend very sensitively on the choices of these options. For cases where no choice is found that avoided failure to achieve a solution, it is not clear whether more flexibility in using TEQ could result in a solution, or if TEQ is not sufficiently realistic to solve for the equilibrium, or if no solution exists in reality. An example of a physics effect not included in TEQ is the full anisotropic pressure caused by the fast particles.

There are several alternative equilibrium solvers available in PTRANSP. One, often used for predictions is VMEC.[19] This is far less accurate in the core. Some of the runs that failed using TEQ are rerun using VMEC for comparisons. The runs completed (past the times where the TEQ runs failed), but significant differences in the computed profiles of the Shafranov shifts, q, and bootstrap currents are seen. Comparisons of the accuracy of the Grad–Shafranov solution and of the calculated I_{BS} are shown in Fig. 8. This indicates the importance of seeking accurate equilibrium solutions, and specifically that the version of VMEC (VMEC6) used in TRANSP and PTRANSP is inadequate for predicting ITER steady state plasmas. Contour plots of the relative error are shown in Fig. 9.

Flux contours calculated for one of the aimings are shown in Fig. 1. Profiles of the elongation and upper and lower triangularity and upper and lower squarenesses are shown in Fig. 10. The definitions of squareness in PTRANSP are the same as in Ref. 7, which shows that increasing negative values of the squareness at the boundary are correlated with increased energy confinement and reduced energy transport in DIII-D steady state plasmas.

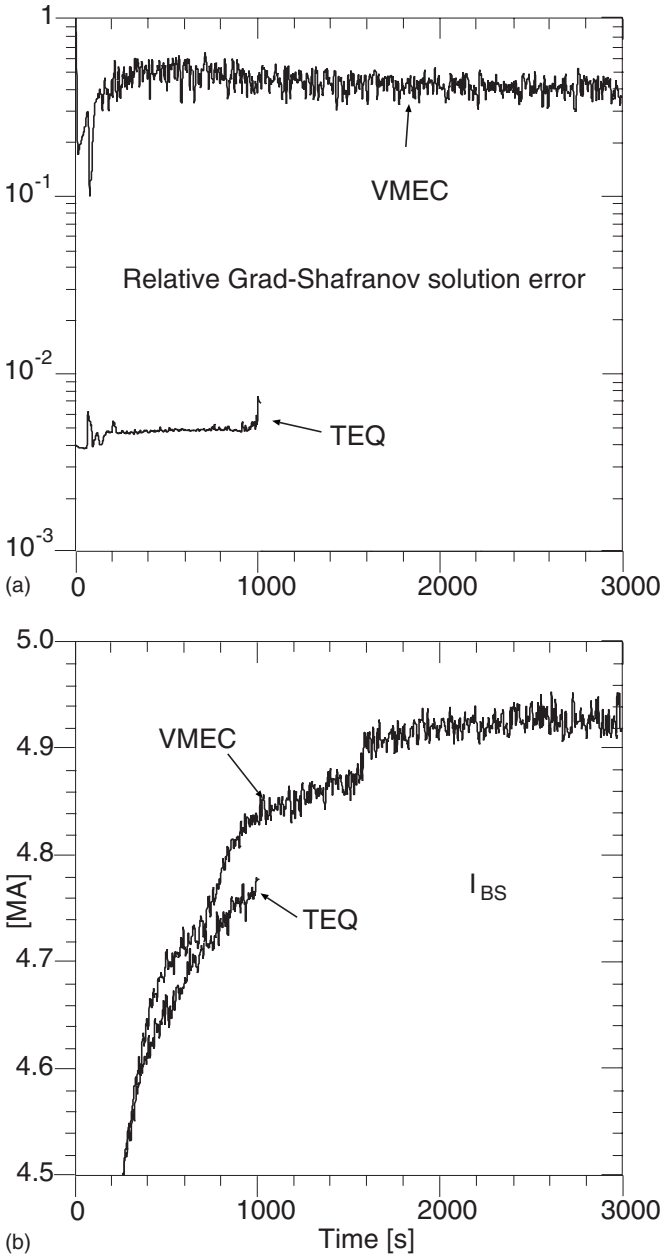

FIG. 8. Comparison of results from two runs identical but for the choice of the Grad–Shafranov solvers VMEC and TEQ showing (a) the relative errors of the Grad–Shafranov equation solutions and (b) the calculated total bootstrap current. The relative error is defined as the surface-averaged magnitude of the difference between the left and right side of the Grad–Shafranov equation normalized by the total. The run using TEQ crashed at 1005 s, whereas the run using VMEC completed to the specified 3000 s.

V. PREDICTIONS FOR TOTAL CURRENTS

The effects on the total NNBI driven current I_{NB} of altering the aiming of the NNBI are mild compared to the changes of their profiles. The current drive efficiency I_{NB}/P_{NB} does not depend strongly on the profile shape, and P_{NB} is held fixed at 33 MW. Ranges of I_{NB} are given in Table I. Results for the Low-T and Low-T-ECCD modes are shown in Fig. 11(a) and for the High-T and High-T-10 modes in Fig. 11(b). The totals are plotted versus both Y the height of the trajectory footprint (the average at the minimum tangency radius) relative to the machine midplane, and Δ the distance relative to the magnetic axis (which is 0.51 m above the vessel midplane). The peak I_{NB} is 70% higher than the lowest value for the Low-T and Low-T-ECCD modes. The increase is less for the High-T and High-T-10 modes. Peak values are obtained near $\Delta = 0.5$ m, i.e., about 0.5 m above the magnetic axis. Note that I_{NB} is asymmetrical with respect to the magnetic axis due to the helicity of the magnetic field.

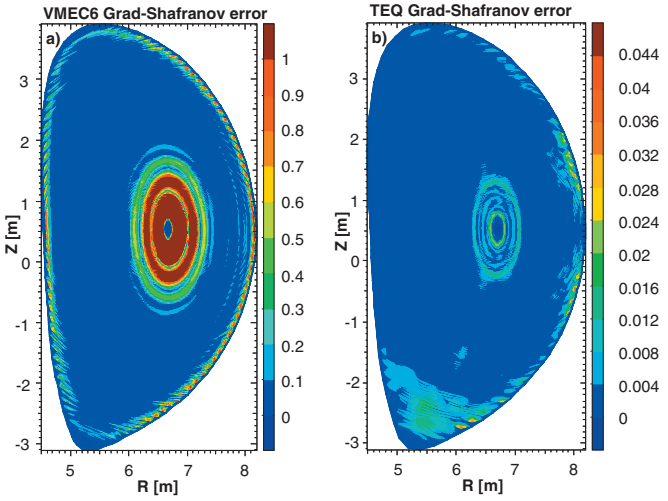

FIG. 9. (Color) Comparison of contour plots of the error of the Grad–Shafranov equation solutions for the two cases shown in Fig. 8; (a) from the run using VMEC shown at 1000 s and (b) from the run using TSC at 1000 s.

The asymmetries in I_{NB} with aiming provide potential advantages of aiming above the magnetic axis.

The bootstrap current is calculated using the NCLASS module[41] in PTRANSP. The total bootstrap current I_{BS}, also shown in Fig. 11 is also asymmetric due to the asymmetric contribution of the beam ion pressure. This pressure alters the Shafranov shift profile, which in turn alters the metric, and the metric alters the gradient of the thermal pressure. This gradient is proportional to the bootstrap current profile. The area-integral of this profile is I_{BS}. The asymmetries in

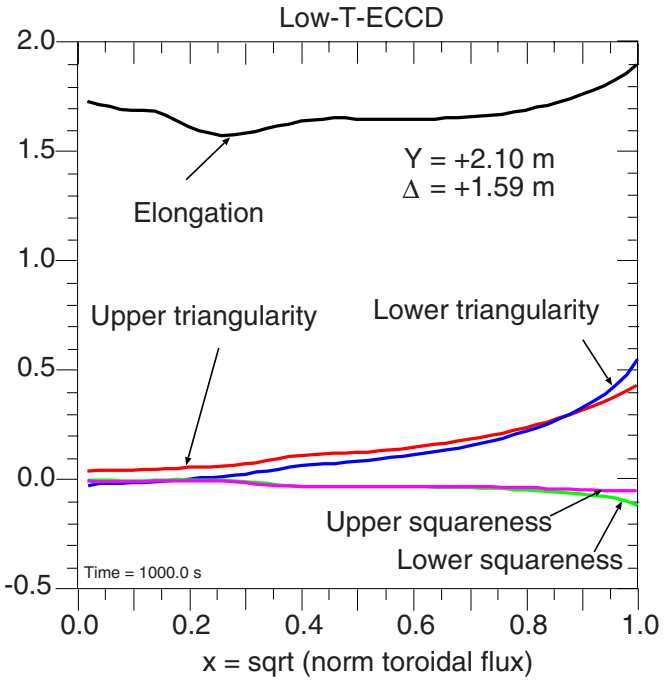

FIG. 10. (Color online) Profiles of the elongation, upper and lower triangularities, and upper and lower squarenesses for one of the Low-T-ECCD mode aimings with footprint height Y=+2.10 m relative to the vessel midplane and Δ=+1.59 m relative to the plasma magnetic axis.

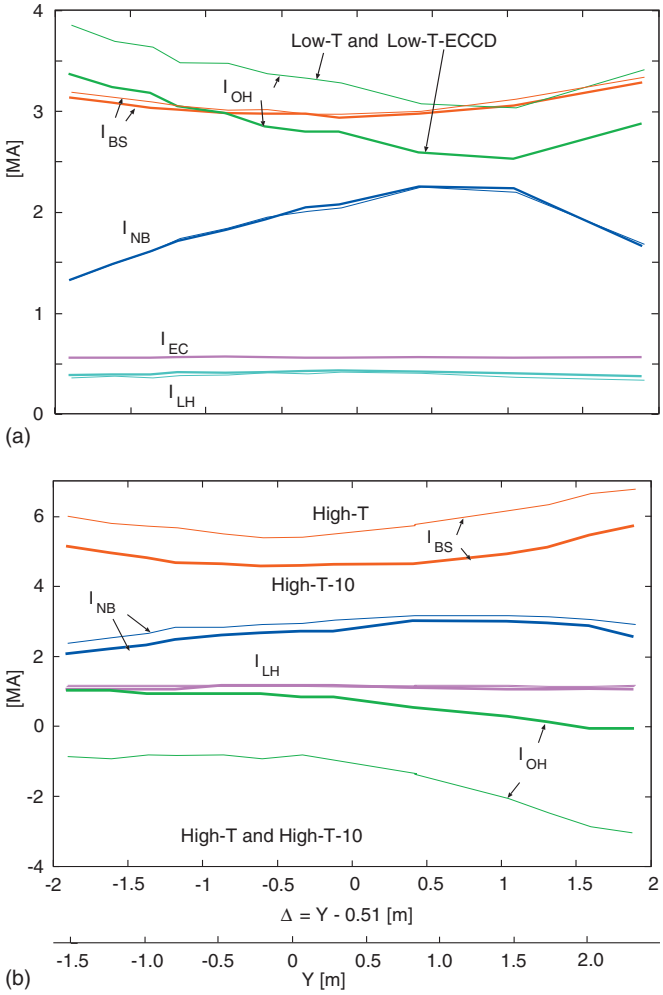

FIG. 11. (Color) Total currents for the a) Low-T (thin) and Low-T-ECCD (thick) and b) High-T (thin) and High-T-10 (thick) modes vs the footprint height and Δ=footprint height minus the height of the magnetic axis. The right-left asymmetry of I_{NB} and I_{BS} in Δ is caused by the helicity of the magnetic field.

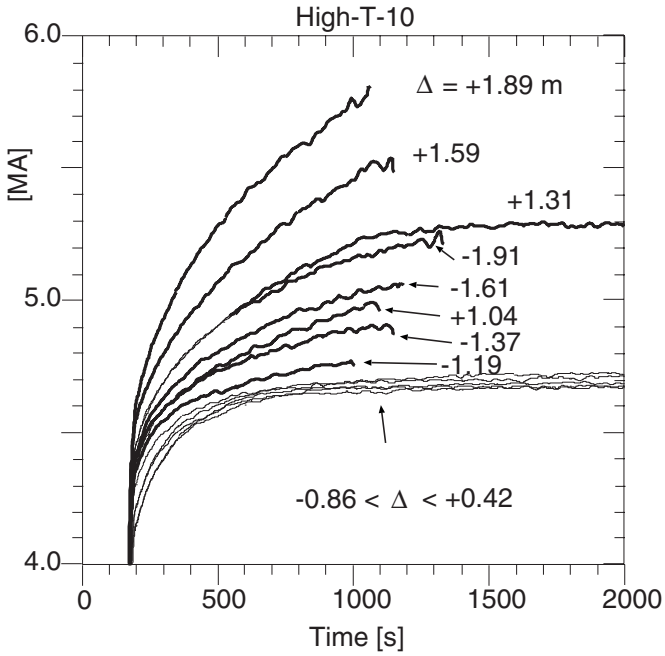

FIG. 12. Evolution of the total bootstrap current for various aimings with the High-T mode.

TABLE II. Summary of results from scans of NNBI aiming for the High-T mode. The aiming angle of the injection below (+) or above (−) the horizontal plane is listed. The height of the footprint is measured relative to the vessel midplane, which is 0.51 m below the computed plasma magnetic axis. Δ is the relative distance between the footprint and axis. The total bootstrap, NNBI, LH, and Ohmic currents are listed at 500 s unless the simulation ended earlier. The flat top termination time is given. Two of the aimings terminated early, due to TEQ not finding a MHD solution to the Grad–Shafranov equation. Current holes defined operationally as q rising above 10 are predicted at least at early times for the aimings for all of the footprint heights.

Steering angle (deg)	Footprint height (m)	Δ (m)	Flat top end (s)	I_{BS} (MA)	I_{NB} (MA)	I_{LH} (MA)	I_{OH} (MA)
−2.10	+2.40	+1.89	500	6.50	2.75	1.15	−1.90
−1.45	+2.10	+1.59	3000	6.40	3.02	1.13	−1.80
−0.97	+1.82	+1.31	3000	6.00	3.10	1.13	−1.60
−0.50	+1.55	+1.04	3000	5.70	3.13	1.15	−1.30
+0.84	+0.92	+0.41	3000	5.45	3.11	1.15	−1.30
+1.81	+0.39	−0.13	176	⋯	3.00	⋯	⋯
+2.30	+0.17	−0.34	500	5.38	2.91	1.15	−0.95
+2.79	−0.10	−0.61	171	⋯	2.90	1.15	⋯
+3.28	−0.36	−0.83	500	5.48	2.80	1.15	−0.85
+3.72	−0.67	−1.21	3000	5.30	2.70	1.15	−0.85
+4.25	−0.86	−1.44	500	5.70	2.62	1.15	−0.85
+4.74	−1.11	−1.61	500	5.78	2.50	1.15	−0.95
+5.23	−1.40	−1.91	500	5.98	2.34	1.15	−0.90

I_{BS} with aiming has a weaker dependence on aiming than that of I_{NB}. Ranges of I_{BS} are given in Table I.

Also shown in Fig. 11 are the total lower hybrid current I_{LH}, electron cyclotron current I_{EC} (for the Low-T-ECCD mode), and Ohmic current I_{OH}. Both I_{LH} and I_{EC} are nearly independent of aiming. However I_{OH} depends on the aiming. It is calculated as the residual current needed to achieve the assumed totals (I_p=9 or 10 MA). The evolution of the Ohmic current profile is calculated assuming neoclassical resistivity (from NCLASS) and Z_{eff}=2.17.

Note that I_{OH} is relatively large for the Low-T and Low-T-ECCD modes [Fig. 11(a)]. One possibility for achieving lower I_{OH} is to lower I_p, although this might lower confinement. Alternatively the driven current could be increased. The High-T and High-T-10 modes assume larger temperatures in order to increase I_{BS}, and also assume higher P_{LH} in order to increase I_{LH}. The lowest magnitude for I_{OH} is near zero for high aiming in the High-T-10 mode, and near unity for low aiming in the High-T mode Fig. 11(b).

Unlike the beam-driven current, the bootstrap current depends strongly on the equilibrium and evolves. Examples of the bootstrap current for the High-T-10 mode are shown in Fig. 12. The total bootstrap is rising steadily even at 500 s, indicating that long flat top durations could be needed to establish steady state. The predictions with large Δ have largest I_{BS} and terminate eventually after 1000 s when PTRANSP-TEQ fail to find a solution to the Grad–Shafranov equation. For these I_{OH} is decreasing toward zero.

TABLE III. Summary of scans in NNBI aiming for the High-T-10 mode. The flat top termination time and I_{BS}, I_{NB}, I_{LH}, and I_{OH} values are listed at 500 s. The aimings that terminated early had increasing I_{BS} at termination.

Steering angle (deg)	Footprint height (m)	Δ (m)	Flat top end (s)	I_{BS} (MA)	I_{NB} (MA)	I_{LH} (MA)	I_{OH} (MA)
−2.10	+2.40	+1.89	1060	5.25	2.64	1.13	0.60
−1.45	+2.10	+1.59	1140	5.10	2.64	1.13	0.50
−0.97	+1.82	+1.89	3000	4.95	2.64	1.13	0.40
−0.50	+1.55	+1.04	1095	4.85	3.08	1.13	0.60
+0.84	+1.00	+0.49	3000	4.70	3.09	1.17	0.60
+1.81	+0.38	−0.13	3000	4.70	2.80	1.24	0.90
+2.30	+0.20	−0.34	3000	4.68	2.80	1.24	1.00
+2.79	−0.08	−0.61	3000	4.70	2.75	1.24	1.10
+3.28	−0.30	−0.83	3000	4.72	2.68	1.24	1.15
+3.72	−0.70	−1.21	1005	4.80	2.56	1.13	1.20
+4.25	−0.93	−1.44	1151	4.85	2.40	1.13	1.30
+4.74	−1.10	−1.61	1179	4.90	2.30	1.13	1.40
+5.23	−1.40	−1.91	1309	4.90	2.15	1.13	1.45

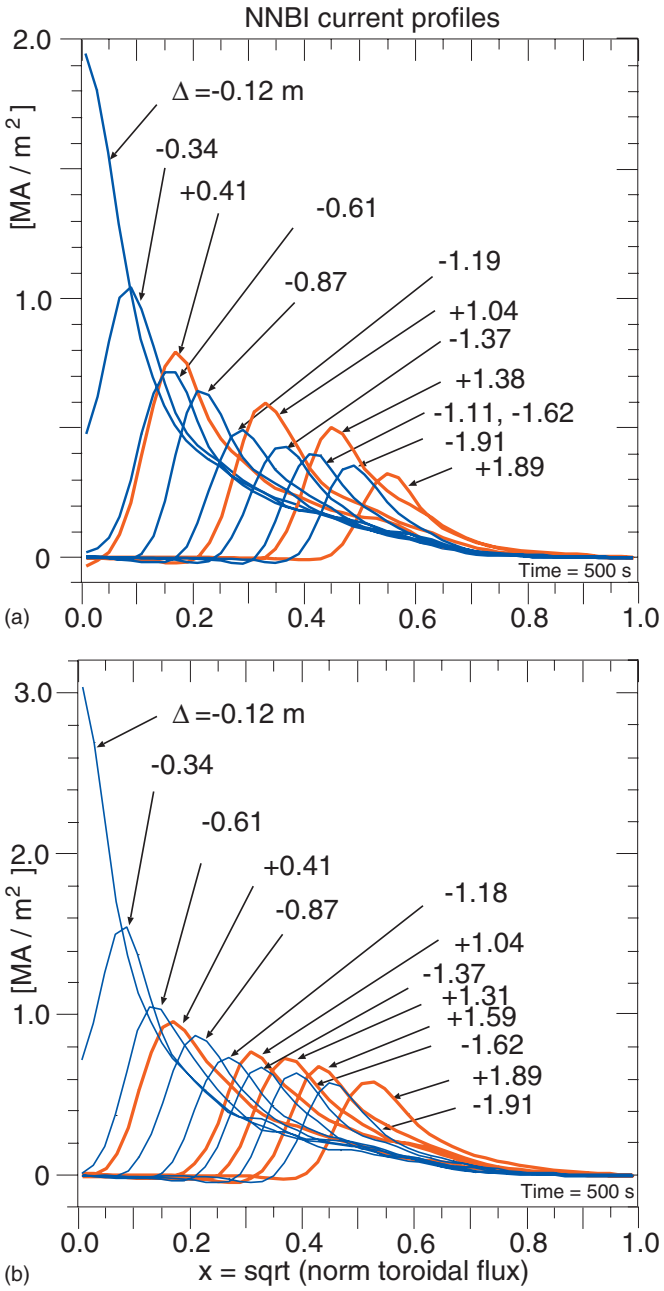

FIG. 13. (Color) Profiles of the NNBI current drive for various aimings of the (a) Low-T and Low-T-ECCD modes and (b) High-T and High-T-10 modes. The profiles with aiming above the magnetic axis (Δ positive) are colored red and those below colored blue.

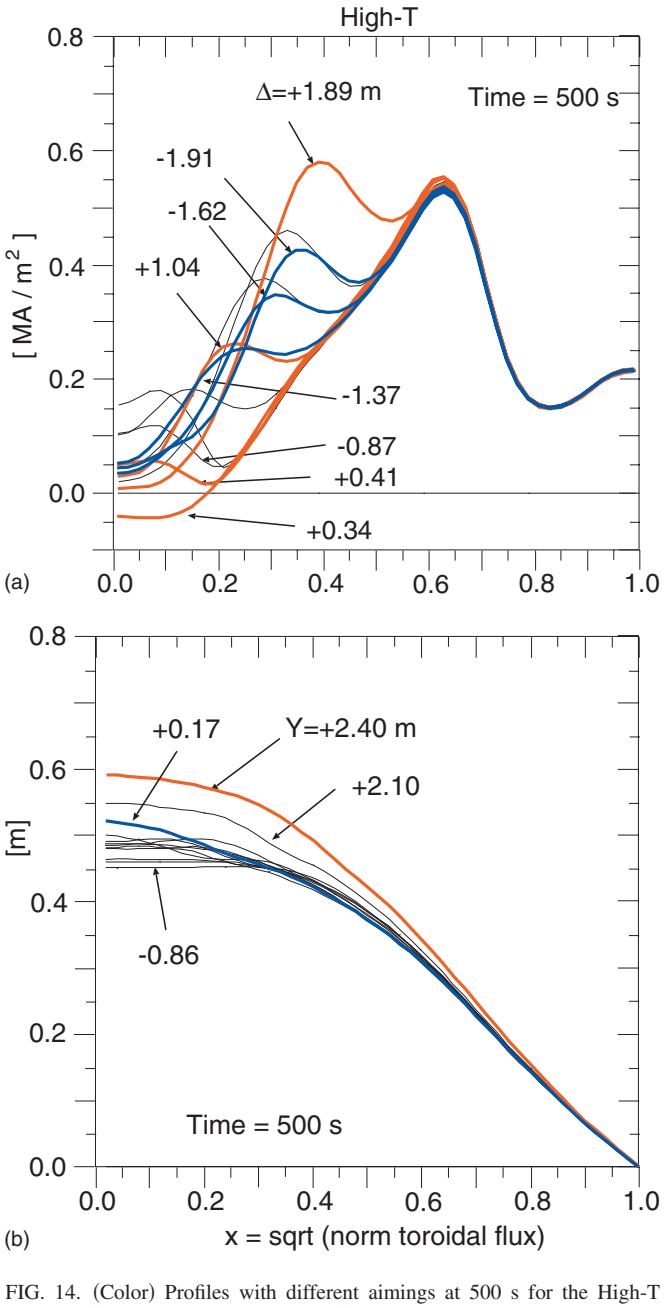

FIG. 14. (Color) Profiles with different aimings at 500 s for the High-T mode of (a) the bootstrap current and (b) the Shafranov shift. The profiles of the bootstrap current have been smoothed over an interval of x=0.1.

Values of I_{BS} at 500 s are shown in Table II. The rates of rise at 500 s are between 1.1 and 3.4 kA/s.

Figure 12 indicates that many of the aimings with large $|\Delta|$ terminate early (before the end set at 3000 s). Termination times are indicated in Table III. These aimings also have low values for $|I_{OH}|$.

VI. PREDICTIONS FOR CURRENT PROFILES

Altering the aiming of the NNBI has strong effects on the beam-driven current profile. Examples for the Low-T mode are shown in Fig. 13(a). As the footprint is raised and the beam-driven current moves inward, peaking on axis with aimings having $\Delta \simeq -0.12$ m. The area-integrated total ($=I_{NB}$) increases to the peak near $\Delta=0.5$ m (above the magnetic axis) shown in Fig. 11(a). With even higher aiming, I_{NB} decreases slightly.

The beam-driven current profiles for the High-T and High-T-10 modes are shown in Fig. 13(b). These profiles are slightly higher than those of the Low-T and Low-T-ECCD modes as a consequence of the increased T_e. Also the bootstrap currents are higher. Profiles of the bootstrap current for the High-T mode (at 500 s) in Fig. 14 show the effects of the beam ion pressure changing the Shafranov shift and thus the gradient of the thermal pressure.

Components of the total current profile for one of the aimings from the Low-T mode scan are shown in Fig. 15. The toroidal currents driven by the pressure gradient and by

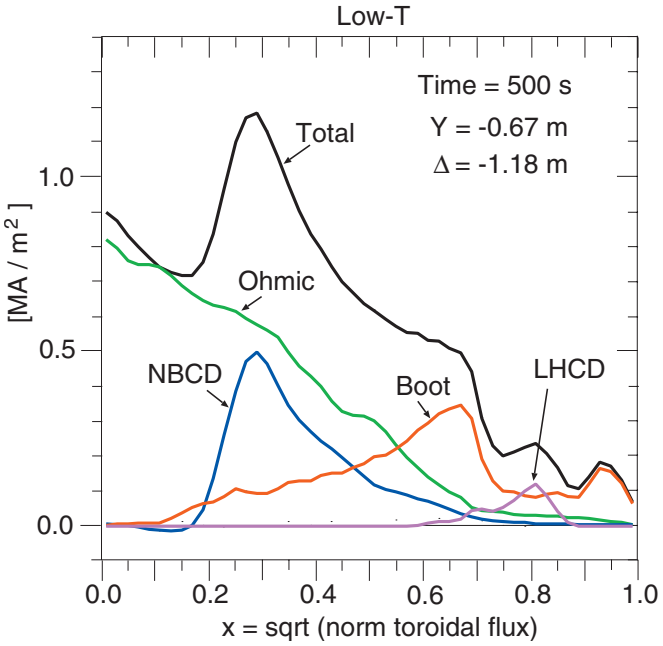

FIG. 15. (Color) Current profile for one case of the Low-T mode.

the fusion ions are also calculated. Their profiles are small and the total of each is about 0.2 kA. Note that a relatively large Ohmic current remains at 500 s.

An example of current profiles for one of the aimings in the Low-T-ECCD mode is shown in Fig. 16. The predicted total ECCD in the Low-T-ECCD mode is 0.55 to 0.60 MW. No optimization of the ECRF launching angles is studied.

An example of current profiles for one of the High-T mode aimings is shown in Fig. 17. The Ohmic current is driven negative in regions around the mid-radius. Since the Ohmic currents computed for the High-T mode are negative, a fourth mode is studied. This is the High-T-10 with the total

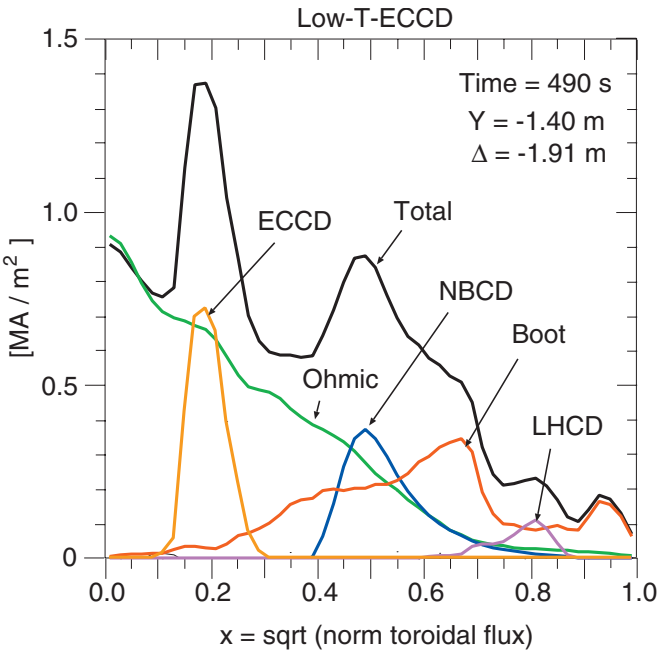

FIG. 16. (Color) Current profiles for one run from the Low-T-ECCD mode.

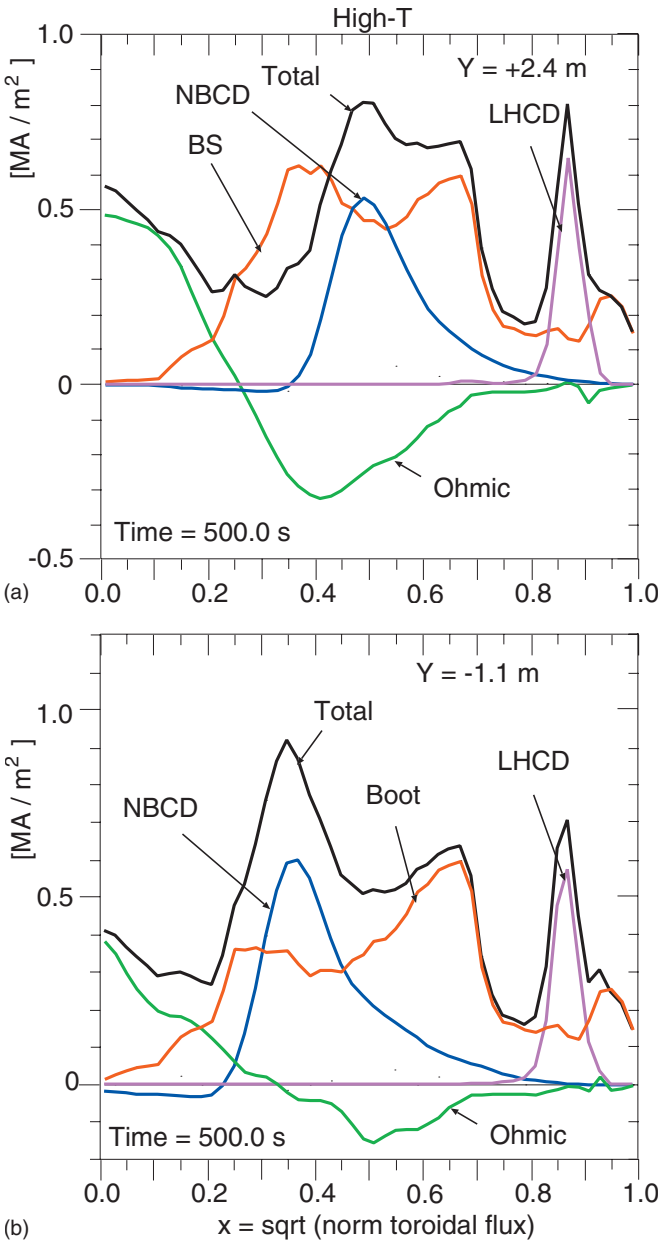

FIG. 17. (Color) Current profiles for two aimings from the High-T mode.

current increased from 9 to 10 MA. Also the flat top time is extended to 3000 s to study slow evolution of the current profiles. Higher I_p decreases q if all else is held fixed. In reality, various other parameters change. For instance, the Shafranov shift is less at higher I_p and the NNBI current drive is shifted outward and the total is reduced slightly. An example of current profiles for one of the High-T-10 mode aimings is shown in Fig. 18. This case was rerun with increased Monte Carlo samples to study the statistical noise. The rerun with 50 000 samples uses parallelized NUBEAM with 16 processors.

VII. PREDICTIONS FOR Q PROFILES

The scan in NNBI steering has weak effects on the q profiles for the Low-T and Low-T-ECCD modes. Examples from the Low-T mode scan are shown in Fig. 19. Such profiles might not have sufficiently high q_{min} and reversal to

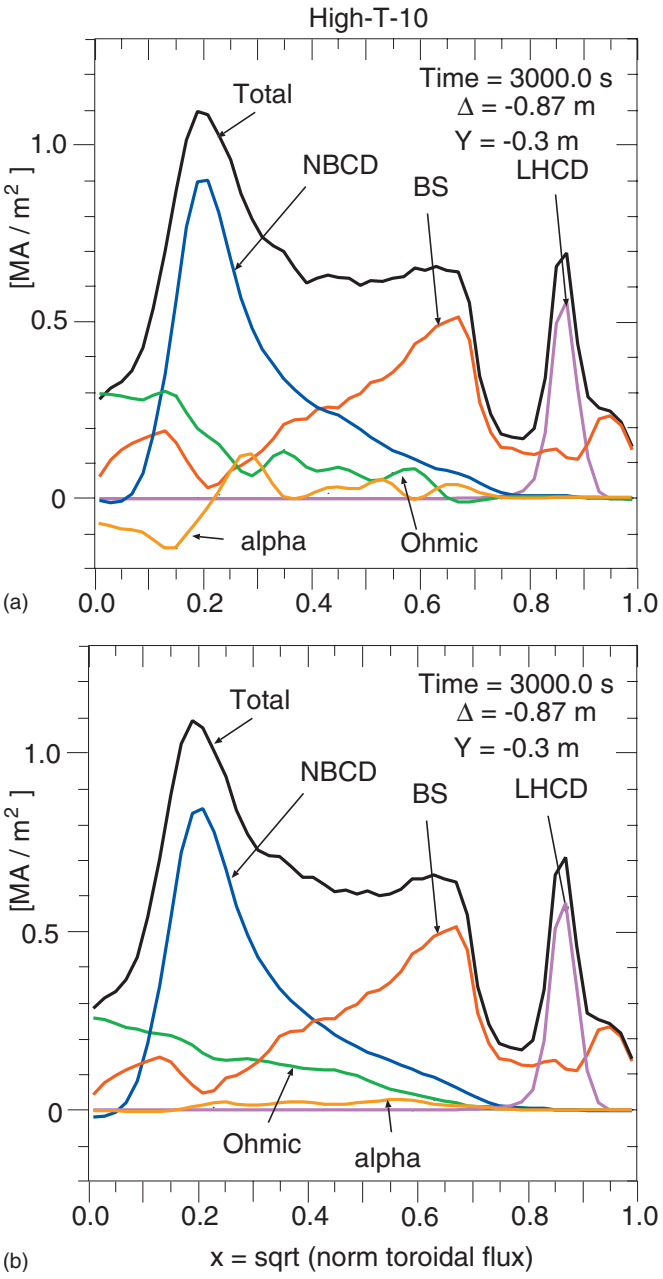

FIG. 18. (Color) Current profiles for one of the aimings from the High-T-10 mode. The number of Monte Carlo samples are varied to compare effects of noise. In (a) 5000 beam and 1000 alpha Monte Carlo particles are used. In (b) 50 000 beam and alpha Monte Carlo particles are used. The profile of the alpha-driven current (analogous to the beam-driven current but from an isotropic DT source) fluctuates in time considerably more in the first case. The time-averages of the alpha-driven currents peak near 0.02 MA/m^2 in both cases.

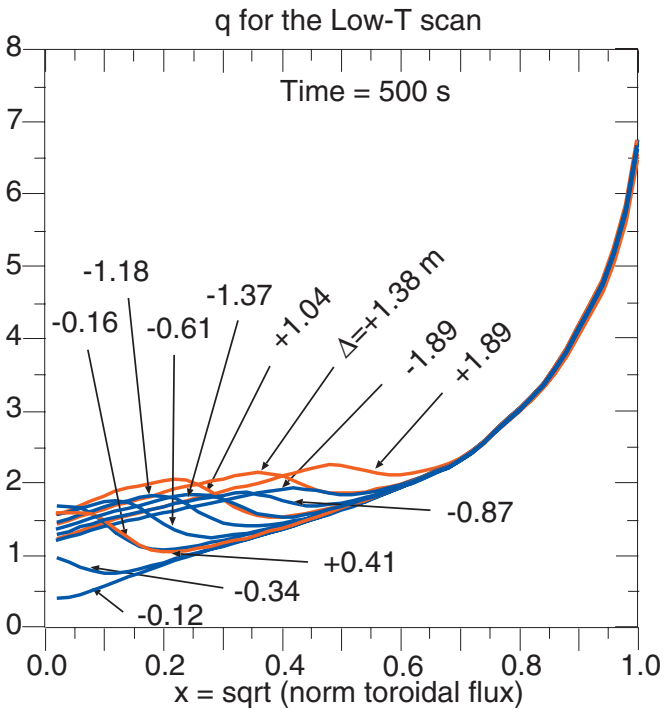

FIG. 19. (Color) Profiles of q at 500 s from the High-T mode. For the runs that continued to the end, the profiles are shown at 500 s.

cause the high performance needed for steady state plasmas. Slightly more reversal is found in the in the Low-T-ECCD mode, as shown in Fig. 20.

A current hole is formed early and disappears by 130 s for one of the Low-T mode aimings ($\Delta=-0.61$ m in Fig. 19). Most of the aimings for the Low-T-ECCD mode start out with current holes, which disappear later. The last by 260 s, for the case with $\Delta=-0.87$ m.

Many of the High-T and High-T-10 mode aimings achieve higher q_{min} and reversal. Figure 21 shows the time evolution of q for two of the aimings in the High-T mode scan. The q profile continues to evolve even after 500 s. Slow evolution to steady state is also predicted for the High-T-10 mode scan. Examples are shown in Fig. 22.

High q_{min} and shear reversal are obtained and maintained in some of the aimings from the scans for the High-T and High-T-10 modes, even up to 2000 s. Examples for the

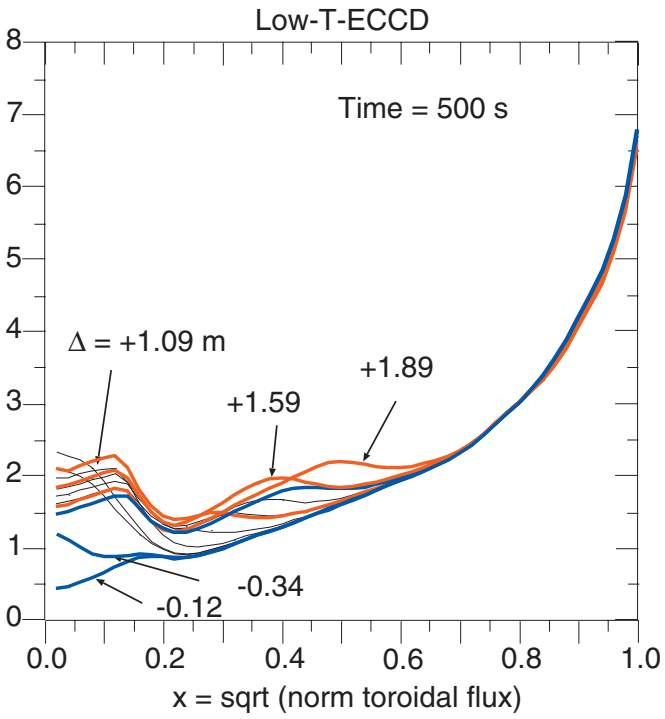

FIG. 20. (Color) Profiles of q at 500 s from the Low-T-ECCD mode.

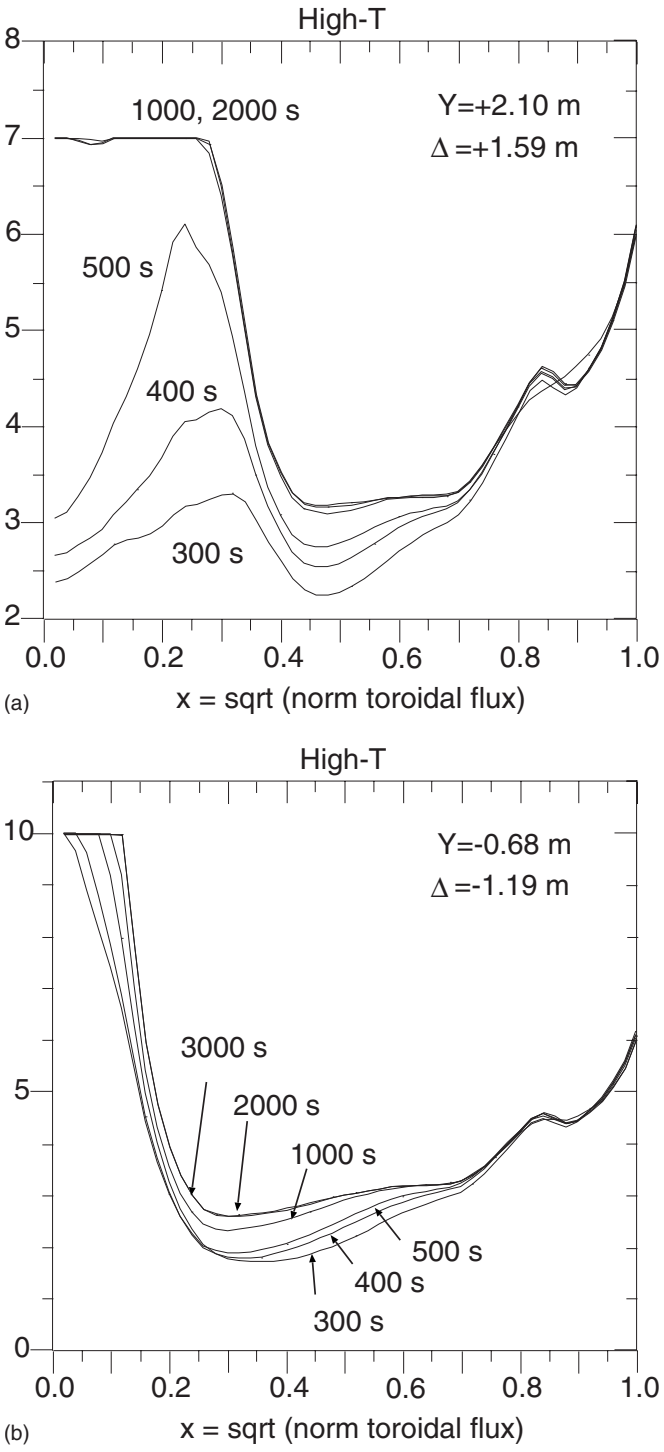

FIG. 21. Evolution of q profiles for two aimings from the High-T mode. For the case with high aiming, a current hole develops by 1000 s. The case with low aiming the current hole persists.

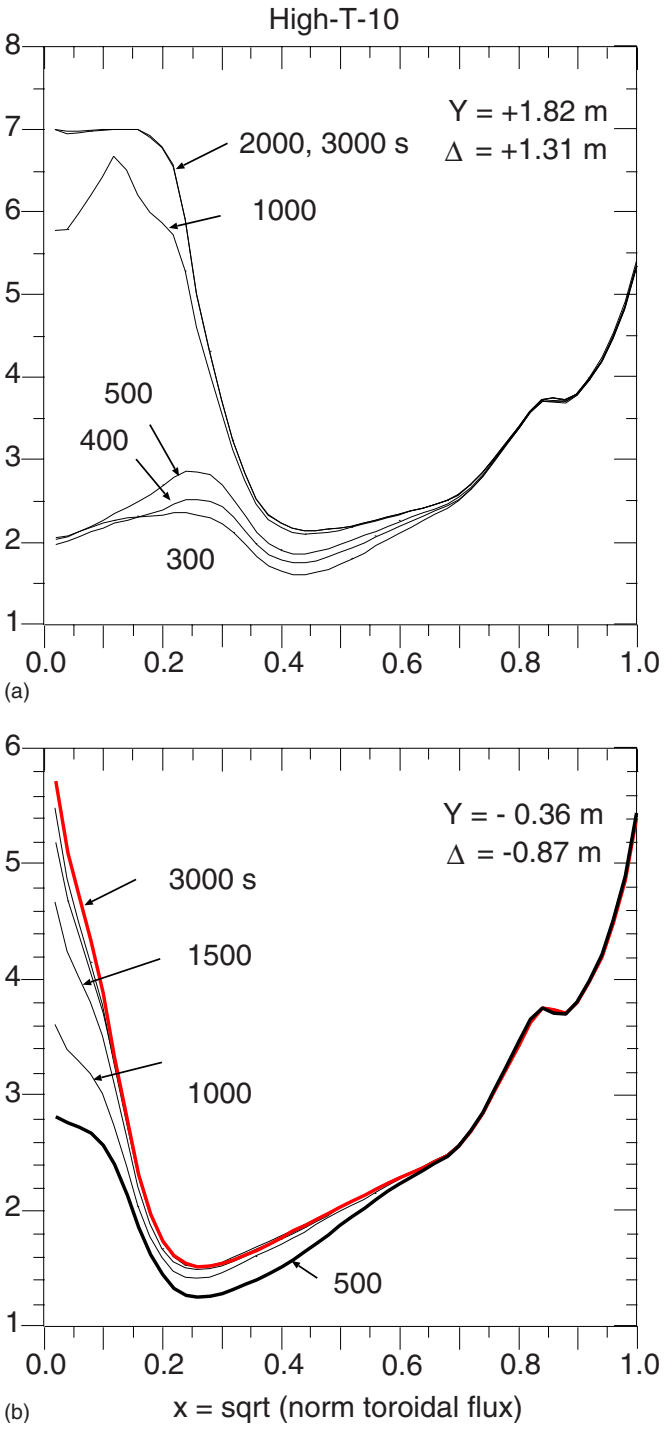

FIG. 22. (Color online) Evolution of q from two of the High-T-10 mode aimings.

High-T mode are shown in Fig. 23. Results from the scans of the High-T-10 mode are shown in Fig. 24. The total bootstrap currents are steady after about 1500 s. The aimings that terminated early all had increasing I_{BS}. The highest rate, 1.2 kA/s is predicted for the case with the highest footprint.

Long-lasting current holes are formed for some of the aimings for the High-T mode. For the one with Y=−0.32 m, the current hole lasts past 500 s. For several, the runs crash, unable to maintain MHD equilibrium. The MHD equilibrium calculations are challenged by high central q and by the beam pressure. Table II gives the termination times for aimings for runs that failed to find equilibria.

To summarize the results for the four modes, the Low-T mode has the highest I_{OH} and mildly reversed q profiles. Most of the aimings result in I_{BS} and q close to steady state conditions after 500 s. All are near steady state by 800 s. None of the aimings challenge the PTRANSP-TEQ equilibrium solver. Only one has a brief current hole early. Several have central q values decreasing below unity.

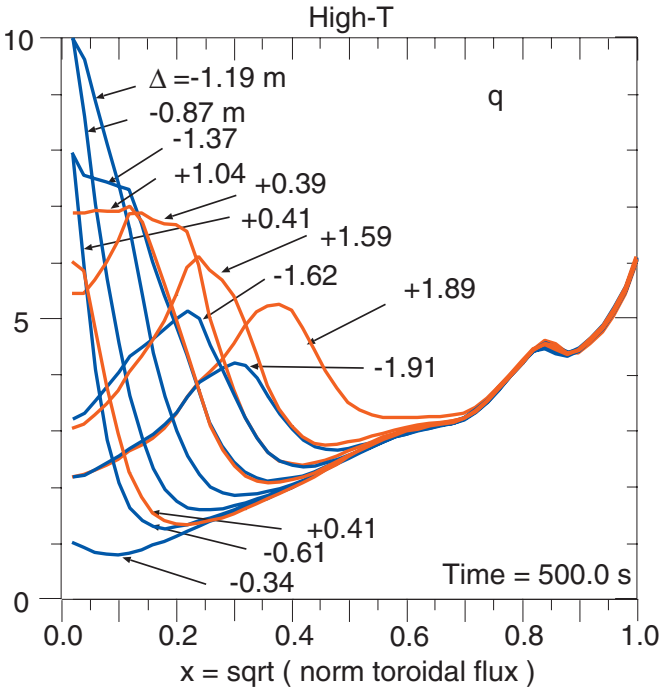

FIG. 23. (Color) Profiles of q from the scans of High-T mode at 500 s.

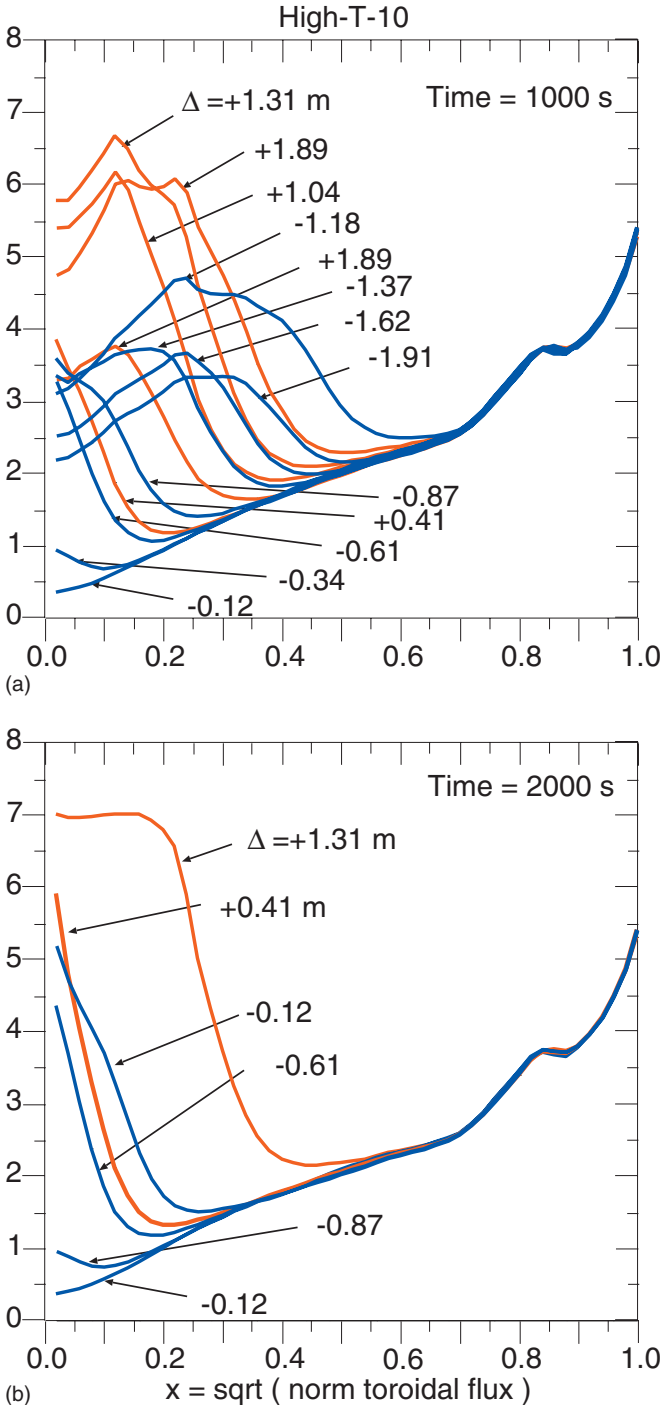

FIG. 24. (Color) Profiles of q from the High-T-10 mode at 1000 and 2000 s. A current hole develops in the run with $\Delta = 1.31$ m after 1000 s, and so the value of q is limited to 7.0.

The Low-T-ECCD mode also has no difficulty running past 500 s and achieves mildly reversed q profiles. Most of the aimings result in I_{BS} and q close to steady state conditions after 500 s. All are near steady state by 800 s. Many of the aimings have current holes, but non lasting past 230 s. Several have central q drooping below unity.

Many of the High-T mode aimings predictions have difficulty maintaining MHD stability. All of the aimings that last for long durations have current holes lasting past 3000 s. Stronger shear reversal and higher q_{min} is achieved. Some of the aimings, especially with low footprints have slow approaches to steady state lasting 1200 s.

The High-T-10 mode has less difficulty with MHD stability than did the High-T mode. They all run past 1000 s, but aimings with high I_{BS} do not come to steady state, and crashed by 1500 s. They have high shear reversal and higher q_{min}.

VIII. DISCUSSION

Quasisteady state, reversed q profiles are predicted in aimings where the driven and bootstrap currents are sufficiently large. The ability to alter the aiming the NNBI aiming is predicted to have large effects on the q profile. In contrast, such steering in ITER standard H-mode plasmas is predicted[16] to not be effective in altering q. This is due to the larger total current assumed (I_p=15 MA), and to the anticipated effects of sawtooth current mixing with large mixing radii.

Since a physics-based predictive model is not used here to establish consistent temperature and density profiles, it is far from certain that the profiles are physical. One test of plausibility is to check if the heat transport appears sufficiently large to be feasible. Profiles of the heat transport χ_e and χ_i for the High-T-10 mode are shown in Fig. 25. Also the neoclassical ion transport χ_{NC} predicted by the NCLASS (Ref. 41) code is shown for comparison with χ_i. The values of χ_i are conservatively higher that χ_{NC}.

An issue generic to LHCD in ITER is how to achieve fueling with pellets since fast electrons from LHCD are found to limit the pellet penetration.[42]

Transients with long durations ($\simeq$1500 s) are predicted. If the plasma profiles were allowed to evolve, the transients would be expected to be even longer. Accurate feedback con-

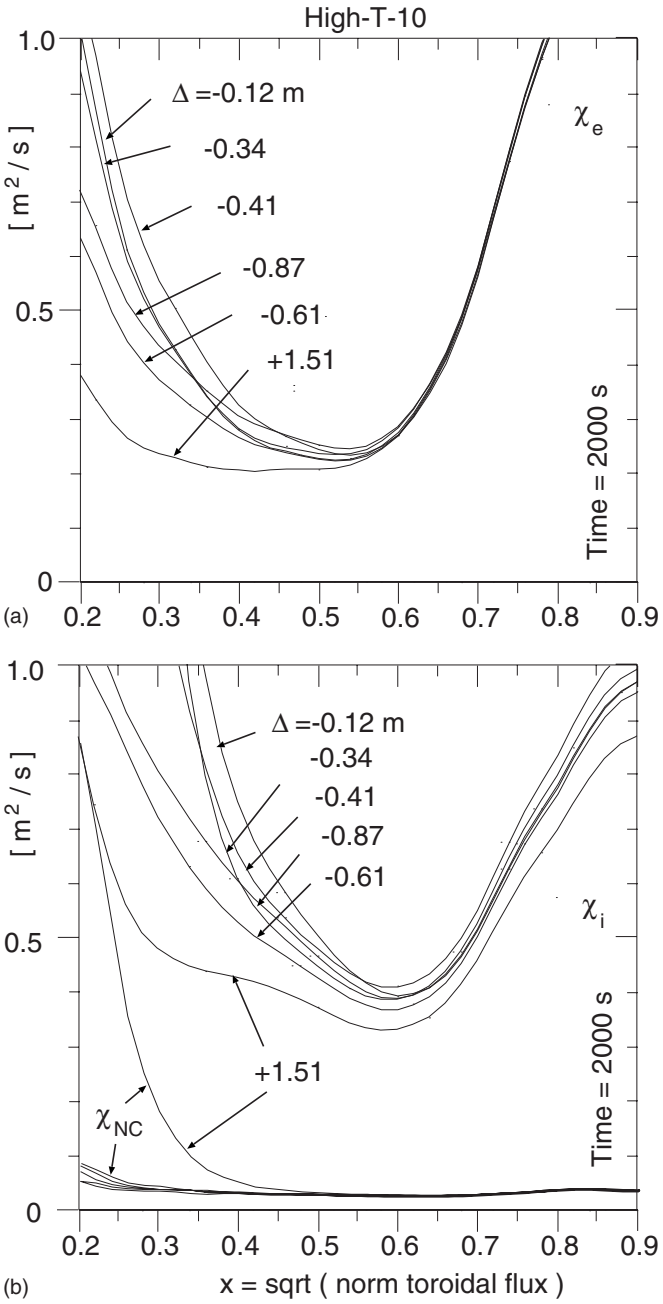

FIG. 25. Profiles of the electron, ion and neoclassical heat conductivity for the High-T-10 mode at 2000 s. The profiles have been smoothed in x. Three of the predictions have central q greater than unity.

trol appears important to direct plasmas to self-consistent steady state conditions within the 3000 s ITER pulse length. Presumably the feedback would require real-time profile measurements of plasma temperatures, densities, heat flows, and q. The actuators could include applied heating and current drive powers, control coil powers, and fueling. Studies of feedback control for ITER steady state plasmas have been published.[43]

The fast ions will also limit pellet penetration, but the density profiles of the fast ions are more central than those expected for the fast electrons. Lastly, achieving MHD stability in ITER steady state plasmas is expected to be challenging. The MHD stability of these predictions has not been investigated.

IX. SUMMARY

The PTRANSP code is used to predict current and q profiles in steady state ITER DT plasmas. Operational modes with either 9 or 10 MA are considered. The boundary (Fig. 1), fixed flat top temperature profiles (Fig. 2), and density profiles (Fig. 4) are assumed. The goals are to find quasi-steady state current profiles, preferably with small Ohmic currents and q profiles with elevated q_{min} and shear reversal since these characteristics appear to be correlated with high performance in present experiments. The current profile actuators explored are NNBI, LHCD, ECCD, and the bootstrap current.

Four modes of operation are considered (summarized in Table I): Low-T and Low-T-ECCD with nominal ITER reference scenario 4 temperature profiles, and High-T and High-T-10 with 50% higher temperatures. All the modes assume 33 MW NNBI. The injection angle is scanned to alter the footprint height in the plasma. All the modes assume LHCD with either 10 or 30 MW. One of the modes (Low-T-ECCD) assumes 10 MW ECCD.

Predictions with elevated q_{min} and shear reversal are shown in Figs. 19–24. Enhancements of the beam-driven and bootstrap currents are predicted with NNBI aiming above the magnetic axis are shown in Fig. 11(b). Transients with long durations ($\simeq$1500 s) are predicted so long duration plasmas may be needed to establish quasistationary q profiles. Only four aimings from the scan in the High-T-10 mode achieve elevated central q after 2000 s, shown in Fig. 24.

The ability to steer the NNBI current and the additional ECCD and LHCD appear to be helpful in controlling the total current profile. Also a high bootstrap current appears to be very helpful, but this contributes to difficulty finding MHD stability.

In some aimings the assumed total current of 9 MA could be too low since the total Ohmic current is negative by up to one MA. Good alignment of the currents with the Ohmic current profile near zero has not been demonstrated here. Presumably active feedback of the current drive will be needed to adjust the profiles in ITER.

Transport is not predicted here. Improved predictive models and integrated modeling are needed to include the dynamical responses of the plasma profiles. The heating profiles are calculated by PTRANSP so the transport implied by the assumed plasma profiles is known. Examples of the electron and ion heat transport conductivities are shown in Fig. 25. The ion heat conductivity is considerably higher that the computed neoclassical ion heat conductivity, suggesting that the plasmas would not require very low levels of transport.

In conclusion, ITER appears poised to study plasmas approaching steady state if it achieves the capabilities of driving and controlling large amounts of current for long durations. Current drive via NNBI, ECRF and LHCD are very desirable for controlling the current profiles. Strong and active feedback appear needed for creating ITER plasmas with conditions close to steady state.

ACKNOWLEDGMENTS

The author wishes to thank R. Andre, R. Goldston, C. Kessel, D. McCune, and S. Zweben for helpful suggestions. The contributions of the PTRANSP development teams at PPPL, Lehigh, GA, and LNL are greatly appreciated. This research is supported by the U.S. Department of Energy under Contract No. DE-AC02-09CH11466.

[1] P.-H. Rebut, M. L. Watkins, D. J. Gambier, and D. Boucher, Phys. Fluids B **3**, 2209 (1991).
[2] R. Aymar, V. Chuyanov, M. Huguet, Y. Shimomura, ITER Joint Central Team, and Home Teams, Nucl. Fusion **41**, 1301 (2001).
[3] X. Litaudon, G. Arnoux, M. Beursken, C. D. Challis, F. Crisanti, P. C. DeVries, C. Giroud, R. A. Pitts, F. G. Rimini, Y. Andrew, M. Ariola, Y. F. Baranov, M. Brix, P. Buratti, R. Cesario, Y. Corre, E. De La Luna, W. Fundamenski, E. Giovannozzi, M. P. Gryaznevich, N. C. Hawkes, J. Hobirk, A. Huber, S. Jachmich, E. Joffrin, H. R. Koslowski, Y. Liang, Th. Loarer, P. Lomas, T. Luce, J. Mailloux, G. F. Matthews, D. Mazon, K. McCormick, D. Moreau, V. Pericoli, V. Philipps, E. Rachlew, S. D. A. Reyes-Cortes, G. Saibene, S. E. Sharapov, I. Voitsekhovitch, L. Zabeo, O. Zimmermann, K. D. Zastrow, and JET-EFDA Contributors, Plasma Phys. Controlled Fusion **49**, B529 (2007).
[4] C. Gormezano, C. D. Challis, E. Joffrin, X. Litaudon, and A. C. C. Sips, Fusion Sci. Technol. **53**, 958 (2008).
[5] M. Murakami, G. M. Greenfield, M. R. Wade, T. C. Luce, J. R. Ferron, H. E. St John, M. A. Makowski, M. E. Austin, S. L. Allen, D. P. Brennan, K. H. Burrell, T. A. Casper, J. C. DeBoo, E. J. Doyle, A. M. Garofalo, P. Gohil, I. A. Gorelov, R. J. Groebner, J. Hobirk, A. W. Hyatt, R. J. Jayakumar, K. Kajiwara, C. E. Kessel, J. E. Kinsey, R. J. La Haye, J. Y. Kim, L. L. Lao, J. Lohr, J. E. Menard, C. C. Petty, T. W. Petrie, R. I. Pinsker, P. A. Politzer, R. Prater, T. L. Rhodes, A. C. C. Sips, G. M. Staebler, T. S. Taylor, G. Wang, W. P. West, L. Zeng, and DIII-D Team, Nucl. Fusion **45**, 1419 (2005).
[6] M. Murakami, M. R. Wade, T. C. Luce, J. R. Ferron, H. E. St. John, J. C. DeBoo, W. W. Heidbrink, Y. Luo, M. A. Makowski, T. H. Osborne, C. C. Petty, P. A. Politzer, S. L. Allen, M. E. Austin, K. H. Burrell, T. A. Casper, E. J. Doyle, A. M. Garofalo, P. Gohil, I. A. Gorelov, R. J. Groebner, A. W. Hyatt, R. J. Jayakumar, K. Kajiwara, C. E. Kessel, J. E. Kinsey, R. J. La Haye, L. L. Lao, A. W. Leonard, J. Lohr, T. W. Petrie, R. I. Pinsker, R. Prater, T. L. Rhodes, A. C. C. Sips, G. M. Staebler, T. S. Taylor, M. A. Vanzeeland, G. Wang, W. P. West, L. Zeng, and DIII-D Team, Phys. Plasmas **13**, 056106 (2006).
[7] C. T. Holcomb, J. R. Ferron, T. C. Luce, T. W. Petri, P. A. Politzer, C. Challis, J. C. DeBoo, E. J. Doyle, C. M. Greenfield, R. J. Groebner, M. Groth, A. W. Hyatt, G. L. Jackson, C. Kessel, R. J. La Haye, M. A. Makowski, G. R. McKee, M. Murakami, T. H. Osborne, J.-M. Park, R. Prater, G. D. Porter, H. Reimerdes, T. L. Rhodes, M. W. Shafer, P. B. Snyder, A. D. Turnbull, and W. P. West, Phys. Plasmas **16**, 056116 (2009).
[8] R. E. Waltz, G. M. Staebler, W. Dorland, G. W. Hammett, M. Kotschenreuther, and J. A. Koning, Phys. Plasmas **4**, 2482 (1997).
[9] W. X. Wang, T. S. Hahm, W. W. Lee, G. Rewoldt, J. Manickam, and W. M. Tang, Phys. Plasmas **14**, 072306 (2007).
[10] M. C. Zarnstorff and S. C. Prager, Phys. Fluids **29**, 298 (1986).
[11] A. R. Polevoi, S. Yu. Medvedev, V. D. Pustovitov, V. S. Mukhovatov, M. Shimada, A. A. Ivanov, Yu. Yu. Poshekhonov, and M. S. Chu, 19th IAEA Conference, Lyon, 2002 (unpublished).
[12] A. Polevoi, A. Zvonkov, T. Oikawa, A. Kuyanov, M. Shimada, A. Saveliev, and Yu. Gribov, Nucl. Fusion **48**, 015002 (2008).
[13] J. García, G. Giruzzi, J. F. Artaud, V. Basiuk, J. Decker, F. Imbeaux, Y. Peysson, and M. Schneider, Phys. Rev. Lett. **100**, 255004 (2008).
[14] J. Garcia, G. Giruzzi, J. F. Artaud, V. Basiuk, J. Decker, F. Imbeaux, Y. Peysson, and M. Schneider, Plasma Phys. Controlled Fusion **50**, 124032 (2008).
[15] W. A. Houlberg, C. Gormezano, J. F. Artaud, E. Barbato, V. Basiuk, A. Becoulet, P. Bonoli, R. V. Budny, L. G. Eriksson, D. Farina, Yu. Gribov, R. W. Harvey, J. Hobirk, F. Imbeaux, C. E. Kessel, V. Leonov, M. Murakami, A. Polevoi, E. Poli, R. Prater, H. St. John, F. Volpe, E. Westerhof, A. Zvonkov, ITPA Steady State Operation Topical Group, and ITPA Confinement Database and Modeling Topical Group, Nucl. Fusion **45**, 1309 (2005).
[16] R. V. Budny, R. Andre, G. Bateman, F. Halpern, C. Kessel, A. Kritz, and D. McCune, Nucl. Fusion **48**, 075005 (2008).
[17] F. D. Halpern, A. H. Kritz, G. Bateman, A. Y. Pankin, R. V. Budny, and D. C. McCune, Phys. Plasmas **15**, 062505 (2008).
[18] R. V. Budny, Nucl. Fusion **49**, 085008 (2009).
[19] S. P. Hirshman, U. Schwena, and J. Nuhrenberg, J. Comput. Phys. **87**, 396 (1990).
[20] C. E. Kessel, G. Giruzzi, A. C. C. Sips, R. V. Budny, J. F. Artaud, V. Basiuk, F. Imbeaux, E. Joffrin, M. Schneider, M. Murakami, T. Luce, H. St. John, T. Oikawa, N. Hayashi, T. Takizuka, T. Ozeki, Y.-S. Na, J. M. Park, J. Garcia, and A. A. Tucillo, Nucl. Fusion **47**, 1274 (2007).
[21] T. Oikawa, J. M. Park, A. R. Polevoi, M. Schneider, G. Giruzzi, M. Murakami, K. Tani, A. C. C. Sips, C. Kessel, W. Houlberg, S. Konovalov, K. Hamamatsu, V. Basiuk, A. Pankin, D. McCune, R. Budny, Y.-S. Na, I. Voitsekhovich, and S. Suzuki, Proceedings of the 22nd International Atomic Energy Agency Conference on Plasma Physics and Controlled Nuclear Fusion Research 2008, Geneva, Switzerland, 13–18 October 2008 (unpublished).
[22] J. E. Kinsey, G. M. Staebler, and R. E. Waltz, Phys. Plasmas **15**, 055908 (2008).
[23] A. Kritz, G. Bateman, R. V. Budny, F. Halpern, D. McCune, A. Y. Pankin, T. Rafiq, and J. Weiland, Proceedings of the 36th EPS Conference on Controlled Fusion and Plasma Physics, Sofia, 2009 (unpublished).
[24] F. Halpern, G. Bateman, A. H. Kritz, R. V. Budny, and J. Weiland, Proceedings of the 36th EPS Conference on Controlled Fusion and Plasma Physics, Sofia, 2009 (unpublished).
[25] J. Weiland, A. Jarmén, and H. Nordman, Nucl. Fusion **29**, 1810 (1989).
[26] R. V. Budny, D. C. McCune, M. H. Redi, J. Schivel, and R. M. Weiland, Phys. Plasmas **3**, 4583 (1996).
[27] R. V. Budny, Nucl. Fusion **42**, 1382 (2002).
[28] M. Murakami, J. M. Park, C. C. Petty, T. C. Luce, W. W. Heidbrink, T. H. Osborne, R. Prater, M. R. Wade, P. M. Anderson, M. E. Austin, N. H. Brooks, R. V. Budny, C. D. Challis, J. C. DeBoo, J. S. deGrassie, J. R. Ferron, P. Gohil, J. Hobirk, C. T. Holcomb, E. M. Hollmann, R. M. Hong, A. W. Hyatt, J. Lohr, M. J. Lanctot, M. A. Makowski, D. C. McCune, P. A. Politzer, J. T. Scoville, H. E. St. John, T. Suzuki, T. S. Taylor, W. P. West, E. A. Unterberg, M. A. Van Zeeland, and J. H. Yu, Nucl. Fusion **49**, 065031 (2009).
[29] R. J. Goldston, D. C. McCune, H. H. Towner, S. L. Davis, R. J. Hawryluk, and G. L. Schmidt, J. Comput. Phys. **43**, 61 (1981).
[30] A. Pankin, G. Bateman, R. Budny, A. Kritz, D. McCune, A. Polevoi, and I. Voitsekhovitch, Comput. Phys. Commun. **43**, 61 (1981).
[31] D. W. Ignat, E. J. Valeo, and S. C. Jardin, Nucl. Fusion **34**, 837 (1994).
[32] C. F. F. Karney and N. J. Fisch, Phys. Fluids **29**, 180 (1986).
[33] D. B. Batchelor and R. C. Goldfinger, Nucl. Fusion **20**, 403 (1980).
[34] A. H. Kritz, H. Hsuan, R. C. Goldfinger, and D. B. Batchelor, 1982 Conference Proceedings of the Third International Symposium on Heating in Toroidal Plasmas ECE, Brussels, Belgium, 1982 (unpublished), Vol. 2, p. 707.
[35] R. Prater, D. Farina, Y. Gribov, R. W. Harvey, A. K. Ram, Y.-R. Lin-Liu, E. Poli, A. P. Smirnov, F. Volpe, E. Westerhof, and A. Zvonkov, and ITPA Steady State Operation Topical Group, Nucl. Fusion **48**, 035006 (2008).
[36] R. Prater, private communication (2009).
[37] V. Pericoli Ridolfini, E. Barbato, A. Bruschi, R. Dumont, F. Gandini, G. Giruzzi, C. Gormezano, G. Granucci, L. Panaccione, Y. Peysson, S. Podda, A. N. Saveliev, FTU Team, and ECH Team, Proceedings of the 14th Topical Conference Radio Frequency Power in Plasmas, Oxnard, California, 2001 (unpublished).
[38] G. Giruzzi, J. F. Artaud, R. J. Dumont, F. Imbeaux, P. Bibet, G. Berger-By, F. Bouquey, J. Clary, C. Darbos, A. Ekedahl, G. T. Hoang, M. Lennholm, P. Maget, R. Magne, J. L. Ségui, A. Bruschi, and G. Granucci, Phys. Rev. Lett. **93**, 255002 (2004).
[39] L. Degtyarev and V. Drozdov, Comput. Phys. Rep. **46**, 481 (1985).
[40] L. L. Lao, H. St. John, R. D. Stambaugh, and W. Pfeiffer, Nucl. Fusion **25**, 1421 (1985).
[41] W. A. Houlberg, K. C. Shang, S. P. Hirshman, and M. C. Zarnstorff, Phys. Plasmas **4**, 3230 (1997).
[42] A. Geraud, C. A. Foster, B. Pegourie, Y. Peysson, P. Bibet, M. Chatelier, H. W. Drawin, and D. Moreau, Proceedings of the 19th EPS Conference on Controlled Fusion and Plasma Physics, Innsbruck, 1992 (unpublished).
[43] D. Moreau and I. Voitsekhovitch, Nucl. Fusion **39**, 685 (1999).